Γ_{CO_2} and calculated T_{surf} as a function of the CO_2 partial pressure p_{CO_2} using results from the radiative-convective model. See the supplementary materials for a definition of all terms and justification of the method.

24. C. H. House, B. Runnegar, S. T. Fitz-Gibbon, *Geobiology* **1**, 15 (2003).
25. C. E. Blank, *Geobiology* **7**, 495 (2009).
26. P. Kharecha, J. Kasting, J. Siefert, *Geobiology* **3**, 53 (2005).
27. Modern ocean net primary productivity is concentrated in shallow regions close to continents (*26*), but in the early Archean, the continental crust volume was about three times lower and the ocean volume may have been up to 25% greater than today (*36, 37*). In the deep ocean away from submarine vents, rates of H_2 supply would be reduced by ~10^3 as compared to the mixed layer, implying a decrease of biological productivity there by a similar factor (*26*).
28. Indirectly, abundant methanogenesis could also have caused global cooling via drawdown of atmospheric N_2.

In atmospheres with 1000 parts per million (ppm) CH_4, atmospheric HCN production rates via photolysis can reach 1×10^{10} cm^{-2} s^{-1} (*38*). Without a mechanism to reform N_2, this could cause the removal of the entire present-day atmospheric N_2 inventory on a time scale on the order of 100 million years.

29. G. M. Young, V. von Brunn, D. J. C. Gold, W. E. L. Minter, *J. Geol.* **106**, 523 (1998).
30. D. J. Stevenson, *Nature* **400**, 32 (1999).
31. R. Pierrehumbert, E. Gaidos, *The Astrophysical Journal Letters* **734**, L13 (2011).
32. R. Wordsworth, *Icarus* **219**, 267 (2012).
33. D. C. Catling, *Science* **311**, 38 (2006).
34. F. Tian, O. B. Toon, A. A. Pavlov, *Science* **311**, 38 (2006).
35. D. S. Abbot, N. B. Cowan, F. J. Ciesla, *Astrophys. J.* **178**, 756 (2012).
36. B. Dhuime, C. J. Hawkesworth, P. A. Cawood, C. D. Storey, *Science* **335**, 1334 (2012).
37. E. C. Pope, D. K. Bird, M. T. Rosing, *Proc. Natl. Acad. Sci. U.S.A.* **109**, 4371 (2012).
38. F. Tian, J. F. Kasting, K. Zahnle, *Earth Planet. Sci. Lett.* **308**, 417 (2011).

Highly Variable El Niño–Southern Oscillation Throughout the Holocene

Kim M. Cobb,[1]* Niko Westphal,[2]† Hussein R. Sayani,[1] Jordan T. Watson,[2] Emanuele Di Lorenzo,[1] H. Cheng,[3,4] R. L. Edwards,[4] Christopher D. Charles[2]

The El Niño–Southern Oscillation (ENSO) drives large changes in global climate patterns from year to year, yet its sensitivity to continued anthropogenic greenhouse forcing is uncertain. We analyzed fossil coral reconstructions of ENSO spanning the past 7000 years from the Northern Line Islands, located in the center of action for ENSO. The corals document highly variable ENSO activity, with no evidence for a systematic trend in ENSO variance, which is contrary to some models that exhibit a response to insolation forcing over this same period. Twentieth-century ENSO variance is significantly higher than average fossil coral ENSO variance but is not unprecedented. Our results suggest that forced changes in ENSO, whether natural or anthropogenic, may be difficult to detect against a background of large internal variability.

The relative strength of the El Niño–Southern Oscillation (ENSO) phenomenon remains one of the most prominent uncertainties in general circulation model (GCM) projections of future climate change (*1*). ENSO is responsible for much of the interannual temperature and precipitation variability across the globe and thus influences energy and water use, ecosystem dynamics, and human health. Consequently, the broad range of ENSO projections represents a fundamental challenge for the development of meaningful climate change adaptation strategies. The uncertainty that arises from comparison of various models is compounded by the fact that instrumental records of ENSO are not sufficiently long to test the accuracy of any given model performance; these records are simply not long enough to provide robust estimates of natural ENSO variability.

Paleo-ENSO records can provide the necessary tests of GCM performance by tracking the response of ENSO to a variety of past natural climate forcings. One prominent example of this approach comes from the mid-Holocene [~6 thousand years (ky) ago] (*2*), an interval when both GCM simulations (*3–6*) and paleo-ENSO reconstructions (*7–10*) show reduced ENSO variability, associated with changes in insolation forcing (*11*). Such data-model agreement seemingly gives credence to the GCMs' abilities to simulate forced changes in ENSO. However, the paleoclimate evidence for a mid-Holocene reduction of ENSO variability is limited—it comprises millennia-long lake or marine sediment records that lack the resolution required to resolve ENSO explicitly (*8–10*), along with several fossil coral sequences that are seasonally resolved but short (*7*). Furthermore, the majority of these records rely on ENSO precipitation responses that may have changed through time.

We analyzed the ENSO variability contained in a collection of monthly resolved, uranium/thorium (U/Th)–dated fossil coral records spanning the past 7 ky from the central tropical Pacific. The archive roughly triples the amount of fossil coral data available to assess ENSO evolution through this time interval. The fossil corals come from Christmas (2°N, 157°W) and Fanning (4°N, 160°W) Islands, located in the Northern Line Islands, which are the site of numerous high-fidelity coral-based reconstructions of 20th-century ENSO spanning the past century (*12–14*) and millennium (*15*). These records allow for quantitative estimates of ENSO variance through time—estimates that can be used to gauge the magnitude of potential forced changes in ENSO variance, both natural and anthropogenic, with respect to natural ENSO variability. Such estimates of natural ENSO variability also provide particularly valuable tests of the long-term ENSO variability exhibited in millennia-long GCM simulations.

Previous work has demonstrated the accuracy and reproducibility of paleo-ENSO reconstructions constructed by using modern and fossil corals from Palmyra Island (6°N, 162°W), which is just north of Christmas and Fanning Islands (*15*). U/Th ages for the 17 fossil coral sequences (7 from Fanning and 10 from Christmas) presented in this study range from 1.3 to 6.9 ky (table S1). Scanning electron microscopy photos reveal evidence for extremely heterogeneous levels of diagenesis, with trace to moderate alteration (<5% by weight) sometimes visible in the same coral (fig. S1 and table S2). Like the modern corals, the fossil coral cores were processed following standard procedures and sampled at 1-mm intervals for oxygen isotopic ($\delta^{18}O$) analyses [long-term reproducibility of $\delta^{18}O$ is ± 0.07 per mil (1σ)] (*16*). The fossil corals' growth rates range from 8 to 20 mm/year, and the records range in length from 19 to 81 years (fig. S2 and table S2).

Northern Line Island coral $\delta^{18}O$ records reflect changes in sea-surface temperature (SST) as well as the $\delta^{18}O$ of seawater (the latter linearly correlated to sea-surface salinity) (*17*), both of which change during ENSO extremes. El Niño events bring warmer and rainier conditions to the Northern Line Islands, conditions which constructively act to decrease coral $\delta^{18}O$ (*12–14*). The opposite climatic effects occur during cool La Niña extremes, driving an increase in coral $\delta^{18}O$. Modern Line Islands coral $\delta^{18}O$ records are highly correlated to the regional-scale NIÑO3.4 index (defined as the average of instrumental SSTs from 5°S to 5°N, and from 120° to 170°W) (Fig. 1). As

[1]School of Earth and Atmospheric Sciences, Georgia Institute of Technology, Atlanta, GA 30332, USA. [2]Scripps Institution of Oceanography, La Jolla, CA 92037, USA. [3]Institute of Global Environmental Change, Xi'an Jiaotong University, Xi'an 710049, China. [4]Department of Earth Sciences, University of Minnesota, Minneapolis, MN 55455, USA.

*To whom correspondence should be addressed. E-mail: kcobb@eas.gatech.edu
†Present address: Department of Earth Sciences, Eidgenössische Technische Hochschule, CH-8092 Zürich, Switzerland.

expected, the magnitude of ENSO-related coral $\delta^{18}O$ anomalies scale with the islands' proximity to the equator. Therefore, in order to assess relative changes in ENSO variance across the entire Line Islands fossil coral collection, we benchmark paleo-ENSO variance in a given fossil coral against late 20th century ENSO variance recorded in the modern coral $\delta^{18}O$ records from the same island.

Our records reveal that ENSO strength has varied substantially over the past 7 ky (Fig. 2A and table S2). In some sequences, interannual variability is statistically insignificant, with reductions of up to –70% (relative to the late 20th century) in 2- to 7-year variance. Such dramatic reductions in ENSO variance occur sporadically throughout the new collection of fossil corals, independently of coral age or preservation. The coral $\delta^{18}O$ reconstructions are broadly consistent with the range of ENSO variance changes contained in existing fossil coral $\delta^{18}O$ reconstructions (7, 18, 19). The expanded collection of fossil coral records shows no systematic shifts in ENSO variance through the mid- to late Holocene. For example, ENSO variance estimates from the mid-Holocene are statistically indistinguishable from those of the past millennium (Fig. 3, A and B). In fact, the only time period that stands out is the 20th century, when ENSO variance estimates are significantly higher than ENSO variance estimates from the Line Islands fossil corals (Fig. 3, C and D), as assessed with a Monte Carlo–based approach that uses 10,000 pairs of pseudocoral time series to assess the significance of observed differences in 2- to 7-year variance (16). However, the high late 20th century ENSO variance is not unprecedented; early 17th century ENSO variance is the highest of the entire Line Islands
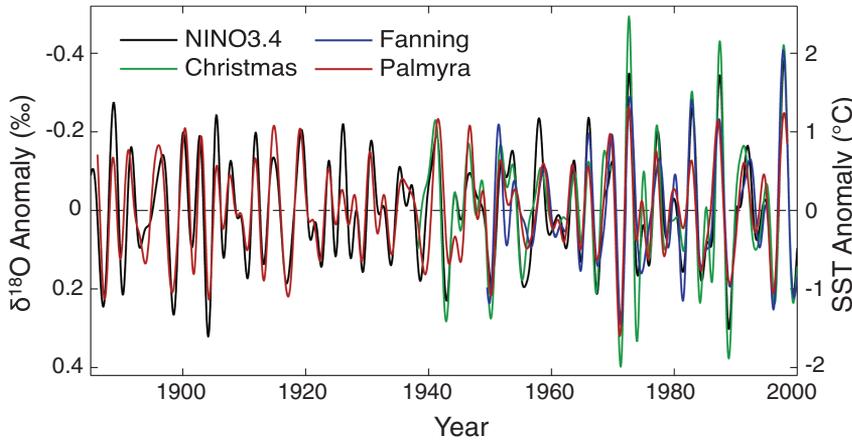

Fig. 1. ENSO variability in Line Islands modern coral $\delta^{18}O$ records and the NIÑO3.4 index [Extended Reconstructed Sea Surface Temperatures, version 3 (ERSST v.3b)] (29). Coral $\delta^{18}O$ data are from Christmas [spliced record constructed from data in (12, 14, 18, 30); (fig. S3)]; Fanning [spliced record constructed from data in (14) and a new Fanning modern $\delta^{18}O$ record (16)] (fig. S4); and Palmyra (13). Each monthly resolved time series has been 2- to 7-year bandpass filtered to highlight ENSO-related variability. Correlation coefficients computed between the bandpassed coral records and the NIÑO3.4 SST index are −0.92, −0.85, and −0.82 for Christmas, Fanning, and Palmyra, respectively.
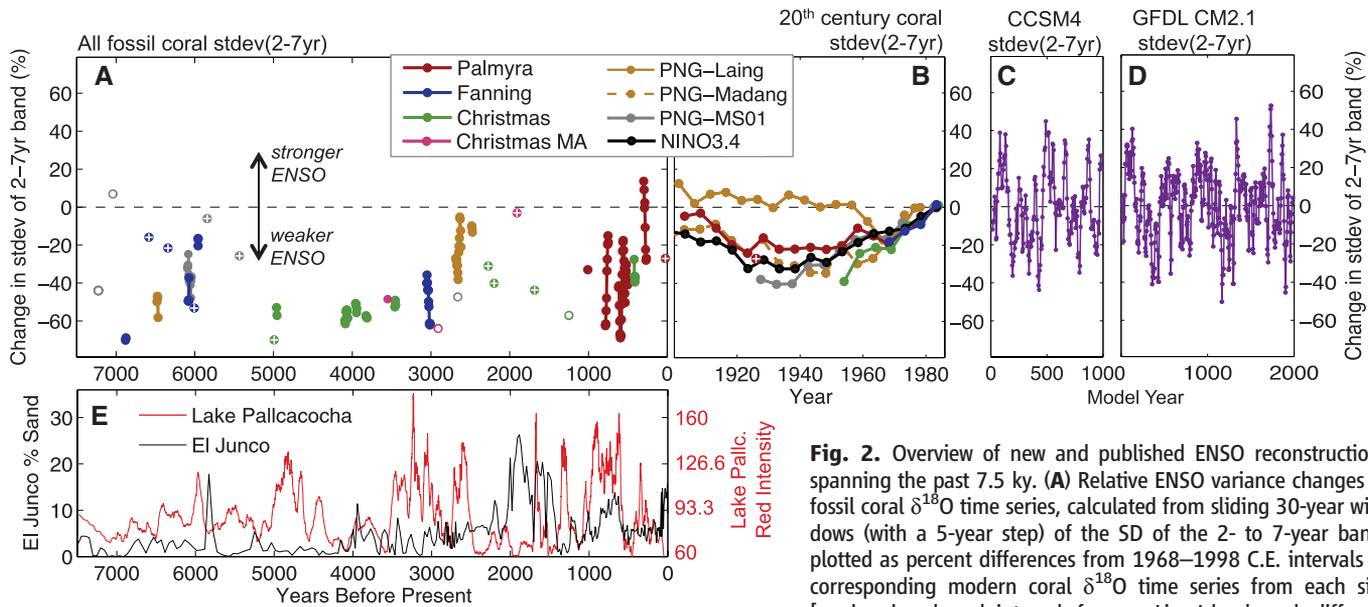

Fig. 2. Overview of new and published ENSO reconstructions spanning the past 7.5 ky. (**A**) Relative ENSO variance changes in fossil coral $\delta^{18}O$ time series, calculated from sliding 30-year windows (with a 5-year step) of the SD of the 2- to 7-year band, plotted as percent differences from 1968–1998 C.E. intervals of corresponding modern coral $\delta^{18}O$ time series from each site [modern benchmark intervals for non–Line Island corals differ by ±5 years (table S3)]. Coral time series with 20 years < length < 30 years are plotted with cross-filled circles. Coral time series with 10 years < length < 20 years are plotted with open circles. Fossil coral $\delta^{18}O$ data are from Christmas Island (green) [this study and (31)]; micro-atolls (pink) (18); Fanning Island (blue) (this study); Palmyra (red) (15); and Papua New Guinea [yellow (7) and gray (19)]. (**B**) Relative ENSO variance changes over the 20th century as recorded in modern coral $\delta^{18}O$ records and the NIÑO3.4 SST index (ERSSTv.3b) (29), calculated from sliding 30-year windows (with a 5-year step) of the SD of the 2- to 7-year bandpassed time series, plotted as percent differences from the 1968–1998 benchmark intervals of the records [modern benchmark intervals for non–Line Island corals differ by ±5 years (table S3)]. Palmyra fossil coral NB9 (15) is replotted here (at date 1926 C.E.) for comparison with the Palmyra modern coral ENSO strength during the early 20th century. Modern coral $\delta^{18}O$ data are from Palmyra (red) (13); Fanning, (blue) (fig S4); Christmas Island (green) (fig. S3); and Papua New Guinea [(yellow (7) and gray (19)]. (**C**) Relative ENSO variance changes in the NCAR CCSM4 1 ky preindustrial control run (23), calculated from sliding 30-year windows (with a 5-year step) of the SD of the 2- to 7-year bandpassed annual NIÑO3.4 time series, plotted as percent differences from the average SD of the entire 2- to 7-year bandpassed model NIÑO3.4 time series. (**D**) Relative ENSO variance changes in the GFDL CM2.1 2 ky preindustrial control run (25), calculated from sliding 30-year windows (with a 5-year step) of the SD of the 2- to 7-year bandpassed monthly NIÑO3.4 time series, plotted as percent differences from the average SD of the entire 2- to 7-year bandpassed model NIÑO3.4 time series. (**E**) Records from Ecuadorian Lake Pallcacocha (red; plotted as an 80-point smooth of the raw red intensity record) (8) and Galapagos Lake El Junco (black; plotted as percent sand fraction) (10).

reconstruction. The choice of a late 20th century benchmark makes the fossil coral ENSO strengths appear anomalously weak, when in fact it is the late 20th century ENSO strength that is anomalously strong.

The coral-based ENSO variance estimates differ appreciably from several lower-resolution records from the eastern equatorial Pacific that have been used to infer sizable mid-Holocene reduc-tions in ENSO variance (Fig. 2E). These archives include two lake sediment records that record fewer El Niño–related flood events in the mid-Holocene (8, 10, 20) as well as a marine sediment record that exhibits a drop in foraminifera pop-ulation variance (reflective of a decrease in annual and/or interannual SST extremes) during the mid-Holocene (9). Differences in the attributes of the various archives (climate sensitivities, chronol-ogy, resolution, and continuity) make it difficult to fully reconcile the divergent views of the Hol-ocene evolution of ENSO. However, instrumental observations suggest that it is possible for east-ern Pacific precipitation anomalies to be muted while central Pacific ENSO variance is relatively strong (21), and the various mid-Holocene ENSO proxies may reflect such geographic complexities. Whatever their origin, the differences underscore the need for rigorous comparison among differ-ent archives, ideally facilitated by translation of tropical Pacific climate variability simulated by models into explicit expectations for proxies (22).

The expanded coral archive does allow for a quantitative assessment of the long-term ENSO variability exhibited by coupled GCMs. The broad range of ENSO variance changes exhibited by the fossil coral database is also characteristic of ENSO variance changes in long, unforced integra-tions of the National Center for Atmospheric Re-search (NCAR)–Community Climate System Model version 4 (CCSM4) (23) and National Oceanic and Atmospheric Administration (NOAA)–Geophysical Fluid Dynamics Laboratory (GFDL)–Climate Model 2.1 (CM2.1) (24, 25) fully coupled GCMs (Fig. 2, C and D, respectively). In the model simulations, NIÑO3.4 variance changes by ±40% (2σ); some centuries-long epochs exhibit large changes in ENSO strength, whereas other epochs feature a relatively stable ENSO. The ENSO variance esti-mates from the Line Islands fossil corals exhibit a similar range of variability, fluctuating by ±36% (2σ) about an average of –42% (with respect to the late 20th century coral benchmark). In fact, the fossil coral ENSO variance distribution is con-sistent with the ENSO variance distribution in models (Fig. 3F), as assessed by subsampling the model time series to match the fossil coral lengths by using a Monte Carlo–based approach (16). The actual Line Islands fossil coral distribution is contained by the spread of the 10,000 pseudocoral realizations, falling well within the 2σ limits of the model distribution.

We conclude that the model data provide a reasonably satisfactory representation of the ENSO variance distribution in the real fossil coral data. The convergence between data-based and model-based estimates of long-term, intrinsic ENSO var-iability suggests that at least some of the current generation of models may accurately simulate long-term changes in ENSO variance, even with-out the inclusion of solar and volcanic natural climate forcings in the models. This data-model agreement suggests that either (i) the models over-estimate unforced ENSO variability or (ii) the natural radiative forcing had little influence on paleo-ENSO variance. In any case, one main im-plication of both the coral- and model-based esti-mates of intrinsic ENSO variability is that the detection (and attribution) of any changes in ENSO properties would require very long time series spanning many centuries, to the extent that de-tection of such changes is even possible (26).

Taken together, the Line Islands fossil coral data suggest that much of the observed differences
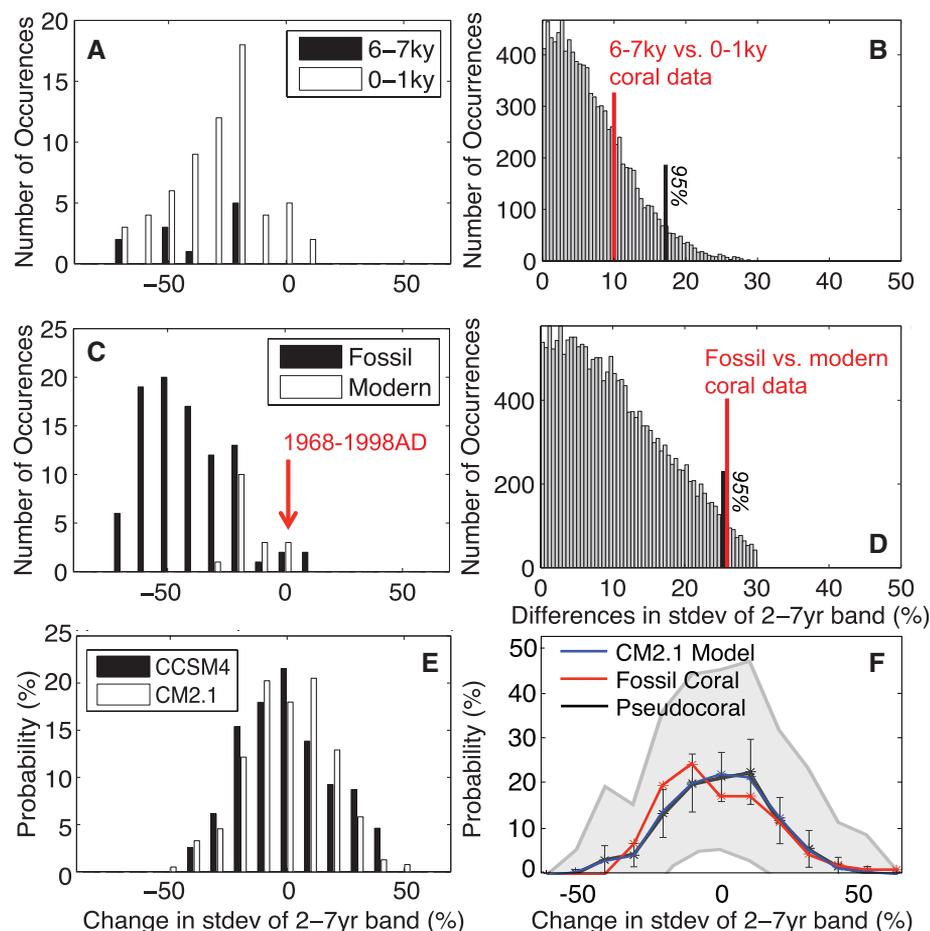

Fig. 3. Comparison of probability density functions of ENSO strength in Line Islands coral data from different time periods, and in model output. (**A**) Distributions of relative ENSO variance changes in Line Islands corals in the 6- to 7-ky interval (black, $n = 193$ years), as compared with the 0- to 1-ky interval (white, $n = 475$ years). (**B**) Significance test of calculated difference between the SD of 2- to 7-year variance in 6- to 7-ky Line Islands corals versus 0- to 1-ky Line Islands corals, as benchmarked using differences calculated from 10,000 "pseudocoral" data sets constructed from the 2-ky-long GFDL CM2.1 NIÑO3.4 time series (16). Red bar indicates the calculated difference between the mean SDs of the 6- to 7-ky and 0- to 1-ky intervals, as compared with the threshold for pseudocoral SD differences significant at the 95% level (black bar). (**C**) Distribution of relative ENSO variance changes in the Line Islands modern coral data (white; the three islands' relative ENSO variance changes as plotted in Fig. 2B have been averaged together to form a composite Line Islands modern coral; $n = 112$ years) and fossil coral data (black; compiled from Fig. 2A; $n = 990$ years). The red arrow marks the late-20th-century ENSO variance benchmark (0% by definition) for the Line Islands corals. (**D**) Same as (B), but for the modern versus fossil coral distributions in (C). (**E**) Distribution of relative ENSO variance changes in the unforced NCAR CCSM4[23] (black) and GFDL CM2.1[25] (white) control runs, compiled from Fig. 2, C and D, respectively. (**F**) Plot of distribution of relative changes of ENSO variance in actual Line Islands fossil coral data (red), as compared with the distribution of 10,000 "pseudo fossil coral" databases compiled by extracting 990 years of GFDL model output in segment lengths corresponding to the actual fossil coral lengths (gray, envelope of individual pseudocoral ensemble distributions; black, pseudocoral mean with 1σ bars), and the dis-tribution of relative changes of ENSO variance from the full 2-ky-long NIÑO3.4 time series from the GFDL model (blue).

in ENSO variance over the past 7 ky reflect strong internal variability. The fact that we detect no discernible influence of orbitally induced insolation forcing on ENSO is noteworthy, given that the effect of insolation forcing on global monsoon circulations is well documented (*27*, *28*). Relatively robust 20th-century ENSO variability may reflect a sensitivity to anthropogenic greenhouse forcing, but definitive proof of such an effect requires much longer data sets than are currently available, given the large range of natural ENSO variability implied by the available fossil coral data.

References and Notes

1. M. Collins *et al.*, *Nat. Geosci.* **3**, 391 (2010).
2. J. Brown, A. W. Tudhope, M. Collins, H. V. McGregor, *Paleoceanography* **23**, PA3202 (2008).
3. B. L. Otto-Bliesner, E. C. Brady, S. I. Shin, Z. Y. Liu, C. Shields, *Geophys. Res. Lett.* **30**, 2198 (2003).
4. Z. Y. Liu, J. Kutzbach, L. X. Wu, *Geophys. Res. Lett.* **27**, 2265 (2000).
5. A. Timmermann, S. J. Lorenz, S. I. An, A. Clement, S. P. Xie, *J. Clim.* **20**, 4147 (2007).
6. W. Zheng, P. Braconnot, E. Guilyardi, U. Merkel, Y. Yu, *Clim. Dyn.* **30**, 745 (2008).
7. A. W. Tudhope *et al.*, *Science* **291**, 1511 (2001).
8. C. M. Moy, G. O. Seltzer, D. T. Rodbell, D. M. Anderson, *Nature* **420**, 162 (2002).
9. A. Koutavas, P. B. deMenocal, G. C. Olive, J. Lynch-Stieglitz, *Geology* **34**, 993 (2006).
10. J. L. Conroy, J. T. Overpeck, J. E. Cole, T. M. Shanahan, M. Steinitz-Kannan, *Quat. Sci. Rev.* **27**, 1166 (2008).
11. A. C. Clement, R. Seager, M. A. Cane, *Paleoceanography* **15**, 731 (2000).
12. M. N. Evans, R. G. Fairbanks, J. L. Rubenstone, *J. Geophys. Res.* **104**, 13409 (1999).
13. K. M. Cobb, C. D. Charles, D. E. Hunter, *Geophys. Res. Lett.* **28**, 2209 (2001).
14. I. S. Nurhati, K. M. Cobb, C. D. Charles, R. B. Dunbar, *Geophys. Res. Lett.* **36**, L21606 (2009).
15. K. M. Cobb, C. D. Charles, H. Cheng, R. L. Edwards, *Nature* **424**, 271 (2003).
16. Materials and methods are available as supplementary materials on *Science* Online.
17. R. G. Fairbanks *et al.*, *Coral Reefs* **16**, S93 (1997).
18. C. D. Woodroffe, M. R. Beech, M. K. Gagan, *Geophys. Res. Lett.* **30**, 1358 (2003).
19. H. V. McGregor, M. K. Gagan, *Geophys. Res. Lett.* **31**, L11204 (2004).
20. D. T. Rodbell *et al.*, *Science* **283**, 516 (1999).
21. K. Ashok, S. K. Behera, S. A. Rao, H. Weng, T. Yamagata, *J. Geophys. Res.* **112**, C11007 (2007).
22. D. M. Thompson, T. R. Ault, M. N. Evans, J. E. Cole, J. Emile-Geay, *Geophys. Res. Lett.* **38**, L14706 (2011).
23. C. Deser *et al.*, *J. Clim.* **25**, 2622 (2012).
24. A. T. Wittenberg, A. Rosati, N. C. Lau, J. J. Ploshay, *J. Clim.* **19**, 698 (2006).
25. A. T. Wittenberg, *Geophys. Res. Lett.* **36**, L12702 (2009).
26. S. Stevenson *et al.*, *J. Clim.* **25**, 2129 (2012).
27. X. Wang *et al.*, *Geophys. Res. Lett.* **34**, L23701 (2007).
28. Y. J. Wang *et al.*, *Nature* **451**, 1090 (2008).
29. T. M. Smith, R. W. Reynolds, T. C. Peterson, J. Lawrimore, *J. Clim.* **21**, 2283 (2008).
30. H. V. McGregor, M. J. Fischer, M. K. Gagan, D. Fink, C. D. Woodroffe, *Geochim. Cosmochim. Acta* **75**, 3930 (2011).
31. L. K. Zaunbrecher *et al.*, *Paleoceanography* **25**, PA4212 (2010).

The Spatial and Temporal Origin of Chandelier Cells in Mouse Neocortex

Hiroki Taniguchi,* Jiangteng Lu, Z. Josh Huang†

Diverse γ-aminobutyric acid–releasing interneurons regulate the functional organization of cortical circuits and derive from multiple embryonic sources. It remains unclear to what extent embryonic origin influences interneuron specification and cortical integration because of difficulties in tracking defined cell types. Here, we followed the developmental trajectory of chandelier cells (ChCs), the most distinct interneurons that innervate the axon initial segment of pyramidal neurons and control action potential initiation. ChCs mainly derive from the ventral germinal zone of the lateral ventricle during late gestation and require the homeodomain protein Nkx2.1 for their specification. They migrate with stereotyped routes and schedule and achieve specific laminar distribution in the cortex. The developmental specification of this bona fide interneuron type likely contributes to the assembly of a cortical circuit motif.

A fundamental issue in understanding cortical circuitry concerns the origin of the identity and diversity of γ-aminobutyric acid–releasing interneurons—basic components of inhibitory circuit organization and assembly. Diverse interneurons regulate the delicate balance and dynamic operation of cortical networks (*1*) and are generated from the medial and caudal ganglionic eminence (MGE and CGE) of the basal ganglia and the preoptic area (*2*). However,

there has been continued debate on what constitutes an interneuron type (*3*) and to what extent the phenotypic descriptions that are used to empirically distinguish cell populations reflect the intrinsic biological processes, such as their developmental specification. This is in part due to the difficulty in tracking the developmental history of any distinct interneurons, from their origin to integration into cortical networks.

Among cortical interneurons, the chandelier cell (ChC) (*4*) displays exceptional stereotypy and specificity: They innervate the axon initial segment (AIS), site of action potential initiation of pyramidal neurons (PyNs) (*5*) and likely represent a bona fide interneuron type. A single ChC innervates hundreds of PyNs and may exert

powerful control over the spiking of a PyN ensemble; thus, together they might constitute a "basic motif" of cortical circuits. However, since their discovery nearly four decades ago, the developmental origin and cortical organization of ChCs have remained elusive.

The homeodomain protein NKX2.1 is specifically expressed by MGE progenitors (*6*). NKX2.1 regulates the formation of the MGE (*6*) and the specification of cortical interneurons (*7*). We found that after the MGE morphologically flattened by about embryonic day 15 (~E15), NKX2.1 expression continued at the ventral germinal zone (VGZ) of the lateral ventricle (Fig. 1, A to C), likely a remnant or extension of MGE, and persisted into the first postnatal week. Along the rostral-caudal axis of VGZ, NKX2.1$^+$ cells were restricted toward the middle-caudal region (Fig. 1, A and C); they expressed progenitor and mitotic markers (Fig. 1C and fig. S1) and incorporated 5-bromo-2′-deoxyuridine (BrdU) (*8*). We generated an *Nkx2.1^{CreER}* knock-in mouse (*8*), with inducible site-specific Cre recombinase (CreER), to achieve a genetic fate mapping of the NKX2.1$^+$ VGZ cells (Fig. 1B), focusing on late gestation and neonatal stages.

A tdTomato red fluorescent protein (RFP) reporter (*9*) induced by tamoxifen on E17 in *Nkx2.1^{CreER};Ai9* embryos labeled radial glialike progenitors along the middle-caudal regions of VGZ (Fig. 1E). VGZ-derived neurons migrated along the lateral wall of the ventricle, reaching the cortex by E18 to postnatal day 0 (P0) (Fig. 1, C, E, and J). Emerging from the dorsal-lateral side of the ventricle wall, migrating neurons split

Cold Spring Harbor Laboratory, Cold Spring Harbor, NY 11724, USA.

*Present address: Max Planck Florida Institute, One Max Planck Way, Jupiter, FL 33458, USA.

†To whom correspondence should be addressed. E-mail: huangj@cshl.edu

Science

Highly Variable El Niño–Southern Oscillation Throughout the Holocene

Kim M. Cobb, Niko Westphal, Hussein R. Sayani, Jordan T. Watson, Emanuele Di Lorenzo, H. Cheng, R. L. Edwards, and Christopher D. Charles

ENSO Variability

The El Niño–Southern Oscillation (ENSO) is the most energetic, quasiperiodic climate oscillation in the world—every few years warming large expanses of the surface equatorial Pacific Ocean surface and impacting temperatures and rainfall patterns across the globe. A pressing question, in the context of global warming, is whether ENSO might be affected by the rising atmospheric temperatures caused by anthropogenic greenhouse gas emissions. Climate models do not agree on the answer to this question, but one place to look for data about how global temperatures might influence ENSO is the record of past ENSO variability. Cobb *et al.* (p. 67) present a record of ENSO variability spanning the past 7000 years, in an attempt better to define its response to insolation forcing over this same period. The findings reveal high variability in ENSO behavior that has no clear dependence on insolation, which implies that a link to warming, if it exists, may be difficult to detect.

View the article online
https://www.science.org/doi/10.1126/science.1228246
Permissions
https://www.science.org/help/reprints-and-permissions